Supplementary Materials for

Conversion of Reactive Carbon Solutions into CO at Low Voltages and High Carbon Efficiency

Zishuai Zhang[1#], Eric W. Lees[2#], Shaoxuan Ren[1], Benjamin Mowbray[1], Aoxue Huang[1], and Curtis P. Berlinguette[1,2,3,4]*

[1]Department of Chemistry, The University of British Columbia, 2036 Main Mall, Vancouver, British Columbia, V6T 1Z1, Canada.

[2]Department of Chemical and Biological Engineering, The University of British Columbia, 2360 East Mall, Vancouver, British Columbia, V6T 1Z3, Canada.

[3]Stewart Blusson Quantum Matter Institute, The University of British Columbia, 2355 East Mall, Vancouver, British Columbia, V6T 1Z4, Canada.

[4]Canadian Institute for Advanced Research (CIFAR), 661 University Avenue, Toronto, M5G 1M1, Ontario, Canada.

[#] These authors contributed equally to this work

*Corresponding author: Curtis P. Berlinguette (cberling@chem.ubc.ca)

Table of contents

Methods **3**

1.1 Faradaic efficiency calculation 3

1.2 Liquid product detection 3

1.3 CO_2 utilization Calculation 4

1.4 Pressurized electrolyser test station 4

2. Technoeconomic analysis **5**

2.1 System description 5

2.2 Input Parameters 6

2.2.1 Electrolyser parameters 6

2.2.2 CO2 capture and separations for the **OER|AEM|CO_2** electrolyser 6

2.2.3 CO2 capture and separations for the bicarbonate electrolyser 7

2.2.4 Hydrogen, electricity, and water consumption 8

2.2.5 Financial parameters 9

2.3 Output parameters 9

2.3.1 Electrolyser sizing 9

2.3.2 Operational expenditures 10

2.3.2.1 Hydrogen, electricity, and water consumption output parameters 10

2.3.2.2 Cost of electricity 10

2.3.2.4 CO_2 capture and separation costs 10

2.3.2.5 Maintenance & water costs 11

2.2.3 Capital expenditures 12

2.2.3.1 Total capex: electrolyser + balance-of-plant 12

2.2.4. Revenue, Profit, and NPV 12

3. Energy consumption analysis (Sankey diagram) **13**

4. BPM and Nafion membrane **13**

4. Supplementary figures **15**

5. References **21**

1. Methods

1.1 Faradaic efficiency calculation

We measured the FE_{CO} at constant current densities (100, 500, and 1000 mA cm^{-2}) by quantifying the H_2 and CO concentrations (for calculating mole fraction of CO in the gaseous mixture analyzed, χ) using a gas chromatograph (GC). The *FE* of a gaseous product k was determined in accordance with Eq. S1[1]:

$$FE_k = \frac{n_k F \chi_k F_m}{I} \quad \text{Eq. S1}$$

Where n_k is the number of electrons exchanged, F is Faraday's constant (F = 96,485 C/mol), F_m is the molar flow rate in mol/s, and I is the total current in A. The molar flow rate is derived from the volume flow rate F_v by the relation $F_m = pF_v / RT$, with p being the atmospheric pressure in Pa, R the ideal gas constant of 8.314 J/mol K, and T the temperature in K.

1.2 Liquid product detection

We used ^{1}H-NMR spectroscopy to identify the concentrations of formate after 20 min of electrolysis at 20 ℃. After the electrolysis using the etched silver foam and bismuth-on-carbon electrodes, a 630-μL aliquot of the circulated catholyte was transferred to an NMR tube and mixed with 70 μL potassium hydrogen phthalate in D_2O with known concentrations as the internal standard. The proton NMR spectra were collected using a 400 MHz spectrometer (Bruker AV400dir) at room temperature. The water signal was suppressed using the Watergate W5 pulse sequence with double gradient echos.[2] A series of standard solutions with known concentrations of formate were prepared and analyzed by ^{1}H NMR, and a calibration curve was created by plotting the relative signal areas versus concentration of formate. From this method, the concentration of formate in the catholyte solution was determined and used to calculate FE_{fomate}. For the electrolysis experiments with silver foam cathode, <1% faradaic efficiency for formate ($FE_{formate}$) was detected.

1.3 CO_2 utilization Calculation

CO_2 utilization was calculated in accordance with Eq. S2. This quantity represents the conversion of *in-situ* generated CO_2 into CO, and therefore, the extent to which the CO is diluted with unreacted CO_2.

$$CO_2\ utilization = \frac{[CO]}{[CO_2]outlet + [CO]}\% \quad \text{Eq. S2}$$

Where [CO] and $[CO_2]_{outlet}$ represent the concentrations of CO and CO_2 in the catholyte headspace as measured by in-line GC analysis.

1.4 Pressurized electrolyser test station

A sealed vessel with a volume of 1 gallon was designed to feed high pressure bicarbonate solution into the bicarbonate electrolyser (Fig. S2). This vessel had 4 ports which were connected to tubing that carried the liquid inlet, liquid outlet, gas inlet, and gas outlet flows. The electrolyte reservoir was filled with 500 mL of 3.0 M $KHCO_3$ solution and the headspace was pressurized by supplying N_2 gas to the gas inlet of the vessel while constricting the outlet gas flow using a pressure regulating valve. The gas flow rate was controlled using a mass flow controller positioned upstream of the reservoir. A pressure relief valve was used to prevent overpressurizing the GC. The pressurized liquid electrolyte was pumped to the electrolyser and continuously recycled to the vessel. Digital pressure indicators positioned at the inlet and outlet of the electrolyser were used to measure the system pressure and pressure drop across the cathode compartment. Gas chromatography measurements were taken after 10 minutes of electrolysis. No liquid products were detected by ^{1}H NMR. Therefore, the FE_{CO} and FE_{H2} were normalized to 100% for every experiment. These normalized FE values obtained at 1 atm with our pressurized bicarbonate electrolyser test station matched that of the experiments performed at ambient conditions, which confirms that the normalized values are accurate. Our rationale behind pressurizing the bicarbonate feedstock pressure, p, was to maximize the concentration of dissolved CO_2 near the catalyst surface. Considering that CO_2 bubbles at the BPM/cathode interface are the main source of CO_2 for bicarbonate electrolyser, we

expected that a higher pressure would increase CO2RR rates by increasing the rate of CO_2 mass transfer from the gas to the electrolyte, R_{MT,CO_2} (Eq. S3).[3]

$$R_{MT,CO_2} = k_{GL,CO_2} M_{CO_2} \left(H_{CO_2} p y_{CO_2} - c_{CO_2(aq)} \right) \quad \text{Eq. S3}$$

Where H_{CO_2} is the Henry's constant for CO_2, y_{CO_2} is the mass fraction of CO_2 in the gas bubbles, and $c_{CO_2(aq)}$ is the CO_2 concentration in the electrolyte. The gas-to-liquid mass-transfer coefficient of CO_2, k_{GL,CO_2}, is given by Eq. S4:

$$k_{GL,CO_2} = \frac{D_{CO_2(aq)}}{\delta_{TF}} \quad \text{Eq. S4}$$

where $D_{CO_2(aq)}$ is the diffusion coefficient of CO_2 in the liquid electrolyte, and δ_{TF} is the thickness of the thin film of electrolyte on the surface of the electrode.[3]

2. Technoeconomic analysis

To benchmark the commercial feasibility of our **HOR|CEM|HCO_3^-** system, we performed a discounted cash flow analysis to compare the 20-year net present value (NPV) of three electrolyser architectures: **HOR|CEM|HCO_3^-**, **OER|BPM|HCO_3^-**, and **OER|AEM|CO_2** electrolysers. This model was developed based on a technoeconomic analysis (TEA) by Jiao and coworkers[4] with modifications that account for the use of bicarbonate and H_2 gas as the cathodic and anodic feedstocks, respectively.

2.1 System description

The focus of the TEA analysis is an electrolyser system which produces 100 ton/day of CO from using either gaseous CO_2 or a bicarbonate solution as the feedstock (Fig. S9). The purpose of the TEA is to determine the potential benefits of pairing bicarbonate electrolysis with HOR instead of OER at the

anode. We used optimistic input parameters for each electrolyser (Table 1) to compare the technologies in a future scenario. We considered a 20-year plant life and a market price for CO of \$0.6/kg[5].

2.2 Input Parameters

2.2.1 Electrolyser parameters

The **HOR|CEM|HCO_3^-** configuration does not suffer from OER overpotentials and therefore enables lower voltages than the **OER|BPM|HCO_3^-** and **OER|AEM|CO_2** electrolyser architectures. In this analyses, the full cell voltages were taken as 2, 4, and 3 volts respectively for the **HOR|CEM|HCO_3^-**, **OER|BPM|HCO_3^-**, and **OER|AEM|CO_2** electrolysers. We assumed that 20% of the CO_2 fed to the bicarbonate electrolyser (in the form of bicarbonate) remains unreacted at the outlet of the bicarbonate electrolyser (i.e., 80% CO_2 utilization). For **OER|AEM|CO_2** electrolyser, the CO_2 utilization value is set as 40% based on our experimental data of bicarbonate electrolysers showing higher CO_2 utilization values, and reports of CO2RR electrolysers which analyze the CO_2 mass flows from laboratory devices.[6] The optimistic FE_{CO} value of 100% at 500 mA cm^{-2} was chosen to demonstrate commercial feasibility in a future setting. An installed cost of \$450/kW was used to determine capital costs associated with the electrolyser.[6]

2.2.2 CO_2 capture and separations for the OER|AEM|CO_2 electrolyser

Based on the control volume in Figure S9a, we determined the upstream CO_2 capture plant capacity using a 1:1 stoichiometric ratio between the molar flow rate of CO in the product stream, $n_{CO,\,formed}$, and the captured CO_2 by absorption, $n_{CO_2,\,absorption}$.

$$n_{CO_2,\,absorptions} = n_{CO,\,formed} \qquad \text{Eq. S5}$$

The downstream CO_2 capture capacity was determined using the molar flow rate of unreacted CO_2 that exits the reactor at steady state.[7–9] Distinct separation processes can be considered for unreacted CO_2

depending on whether the CO_2 exits at the anode (via a CO_2 crossover mechanism) or the cathode (Figure S9a).[6] However, an industrial benchmark for CO_2 separations has not been established for CO2RR electrolysers. We therefore did not consider cost differentials between the CO_2 capture and CO_2 separation units. For simplicity, we used a gross CO_2 capture cost of $50/ton for both CO_2 capture and separation.

Figure S9a shows that the inlet molar flow rate to the **OER|AEM|CO_2** electrolyser consists of two "cathode in (pure CO_2)" streams which come from either CO_2 absorption or CO_2 separation steps. These two CO_2 feed streams have a combined molar flow rate that is equal to the sum of the CO_2 captured by absorption, $n_{CO_2,\,absorbed}$, and the CO_2 separated downstream of the reactor, $n_{CO_2,\,separated}$. Consequently, a mass balance on the electrolyser yields the following expression for $n_{CO_2,\,separated}$,

$$n_{CO_2,\,separated} = (\frac{1}{x} - 1)n_{CO,\,formed} \quad \text{Eq. S6}$$

where x represents the CO_2 utilization efficiency which relates the molar product of CO to the CO_2 feedstock.

$$x = \frac{n_{CO,\,formed}}{\Sigma n_{CO_2,\,inlets}} \quad \text{Eq. S7}$$

Note that $n_{CO_2,\,separated}$ represents the total downstream CO_2 separation requirement which can be fulfilled using a combination of CO_2 absorption or CO_2 separation capacity (note the two recycle streams shown in Fig. S9a for the **OER|AEM|CO_2** electrolyser). For the 100 ton/day facility under investigation, a single pass conversion value of 40% corresponds to 149 kmol/h of CO_2 captured and 223 kmol/h of CO_2 separated after the electrolyser.

2.2.3 CO_2 capture and separations for the bicarbonate electrolyser

Bicarbonate electrolysis can bypass CO_2 regeneration in the CO_2 capture process (Figure S6b).[10] Therefore, we estimated the cost of CO_2 capture from flue gas without CO_2 regeneration to determine the cost of the bicarbonate electrolysis pathways. CO_2 regeneration constitutes ~80% of the operating costs

of CO_2 capture due to the large associated heat duty in the reboiler.[11] However, CO_2 regeneration only accounts for 21% of capital costs because the stripper and reboiler units are much less expensive than the absorber.[12] Based on these assumptions, the cost of CO_2 from bicarbonate ($C_{CO_2\ from\ bicarbonate}$) is expected to have 20% of the operating expenditures and 79% of the capital expenditures of an equivalent system that supplies gaseous CO_2 to an electrolyser,

$$C_{CO_2\ from\ bicarbonate} = 0.2C_{CO_2\ gas,\ opex} + 0.79C_{CO_2 gas,\ capex} \quad \text{Eq. S8}$$

In order to determine the total cost of CO_2 from bicarbonate, we estimated that the operating costs constitute 71% of the total costs of CO_2 capture.[13] On this basis, we determined that eliminating CO_2 regeneration by use of a bicarbonate feedstock could reduce the supply cost of CO_2 from air or flue gas by a factor of 0.37 (Eq. 9)[14]:

$$0.2(0.71C_{CO_2,\ total}) + 0.79(0.29C_{CO_2,\ total}) = 0.37C_{CO_2,\ total} \quad \text{Eq. S9}$$

This cost reduction parameter is considered optimistic. Detailed TEA and process modeling work is needed to more accurately define this parameter, but such work is beyond the scope of this study. It is important to note that the cost reduction parameter was used to exclusively determine the CO_2 capture cost. CO_2 separation costs incurred downstream of the bicarbonate electrolyser were calculated using the same procedure as for CO2RR electrolysers (Section 2.2.2).

2.2.4 Hydrogen, electricity, and water consumption

In our TEA analysis we set the cost of hydrogen as \$1/kg to represent the target that the recent DOE EarthShot initiative seeks to achieve in 10 years.[15] We assumed a 100% FE for HOR at the anode. The electricity price was assumed to be \$0.03/kWh based on projections for renewable electricity costs in 2030[16] and the water price was assumed to be \$0.0054/gallon[5].

2.2.5 Financial parameters

Other conditions that affect financial outcomes are briefly decreased here: the net present value (NPV) was calculated using a discounted cash flow analysis with a nominal interest rate of 10% and an income tax rate of 38.9%. As per the DOE's H2A analysis for water electrolysis[17], a modified accelerated cost recovery system (MACRS) was used with a working capital equal to 5% of the capital costs and a 10-year depreciation lifetime with a 20% salvage value at the end of 20 years. All dollar values are reported in present-day US dollars.

2.3 Output parameters

2.3.1 Electrolyser sizing

The total electrode area was determined directly based on the CO product formation rate (100 ton/day) and the current density (500 mA cm^{-2}) using Faraday's law of electrolysis (Eq. S10)

$$S_{electrode} = \frac{required\ CO\ production\ rate}{unit\ CO\ formation\ rate\ at\ cathode} \quad \text{Eq. S10}$$

A CO production rate of 100 ton/day corresponds to a molar flow rate of 149 kmol h^{-1}. This value constitutes the basis for all mass balance calculations. Therefore, a total electrode area of 1594 m^2 was calculated for each electrode based on the same current density (500 mA cm^{-2}) and FE_{CO} (100 %) values. Power consumption was calculated using the voltage and current of the electrolyser (Eq. S11),

$$Power = j \times S_{electrode} \times V_{cell} \quad \text{Eq. S11}$$

where j represents the operating current density (500 mA cm^{-2}) and V_{cell} represents the full cell potentials.

2.3.2 Operational expenditures

2.3.2.1 Hydrogen, electricity, and water consumption output parameters

The total amount of H_2 used for the **HOR|CEM|HCO_3^-** electrolyser was determined based on the electrode area, the CO formation rate, and the HOR stoichiometry as follows:

$$H_{2(g)} + CO_{2(g)} \rightarrow CO_{(g)} + H_2O_{(l)} \quad \text{Eq. S12}$$

From this equation, the total H_2 consumed in the **HOR|CEM|HCO_3^-** electrolyser was determined to be 7 ton/day. The corresponding H_2 cost was determined to be 2.61 M/year based on the $1/kg target price for H_2 in the DOE's EarthShot.[15] The amount of water used for each of the **OER|BPM|HCO_3^-** and **OER|AEM|CO_2** electrolysers was determined based on the OER stoichiometry (Eq. S13):

$$H_2O\ flow\ rate(mol/s) = \frac{j \times S_{electrode}}{Z \times F} \times \frac{0.018\ kg}{mol} \times \frac{2642\ gal}{kg} \times \frac{86400\ s}{day} \quad \text{Eq. S13}$$

Z represents electron transfer number (z = 4 for OER), and F represents Faraday constant (96485 C/mol).

2.3.2.2 Cost of electricity

The total current and FE_{CO} is the same for each electrolyser pathway and therefore cell potential is the only electricity cost factor that varies between the different electrolyser pathways. The **HOR|CEM|HCO_3^-** system had the lowest electricity cost ($8.4 M) and the lowest cell potential (2 V), followed by the **OER|AEM|CO_2** electrolyser with $6.3 M and 3 V, and the **OER|BPM|HCO_3^-** electrolyser with $8.4 M and 4 V.

2.3.2.4 CO_2 capture and separation costs

In the CO2RR, 1 mole of CO is produced for every 1 mole of CO_2 that is electrochemically reduced (assuming that CO is the only CO2RR product). Therefore, a total mass of 157 tons CO_2 is needed to produce 100 tons of CO based on a ratio of the molecular weights of CO and CO_2. To determine

the CO_2 capture costs for the **OER|AEM|CO_2** electrolyser, a cost of $50/ton was used. To estimate the cost of CO_2 from bicarbonate, an optimistic cost reduction parameter of 0.37 was used to reflect cost savings associated with eliminating CO_2 regeneration (details in 2.2.2). The annual CO_2 capture costs for the **OER|AEM|CO_2** electrolyser were determined to be 2.9 $M/year, which is higher than the bicarbonate electrolyser configurations (1.06 $M/year), which do not require CO_2 regeneration.

Unreacted CO_2 was assumed to be separated from the product stream at a cost of $50/ton for all electrolyser pathways. Costs associated with separating unreacted CO_2 electrolysis were estimated using the methodology described in Section 2.2.2 for both the **OER|AEM|CO_2** and bicarbonate electrolysers. The total CO_2 separated from the product stream was determined based on the single pass conversion or CO_2 utilization. The bicarbonate electrolyser configurations were assumed to have higher CO_2 utilizations and therefore required low CO_2 separation costs (0.75 $M/year) than the **OER|AEM|CO_2** electrolysers (4.3 $M/year). A major reason that **OER|AEM|CO_2** electrolysers were found to have high CO_2 separation costs is the carbonation problem, which causes CO_2 reactant to crossover to the anode and mix with O_2 from the OER.[6,18] The total CO_2 capture and separation costs associated with the bicarbonate electrolysers (**HOR|CEM|HCO_3^-**, **OER|BPM|HCO_3^-**) were estimated at 1.8 $M/year. The value for the **OER|AEM|CO_2** electrolyser value was higher (7.2 $M/year) because of CO_2 regeneration costs and a lower CO_2 utilization (single pass conversion) value.

2.3.2.5 Maintenance & water costs

Maintenance costs were assumed to be 2.5% of the electrolyser capital expense and water costs were assumed to be $0.0054/gal.[5] The **HOR|CEM|HCO_3^-** system does not consume water for electrolysis.

2.2.3 Capital expenditures

2.2.3.1 Total capex: electrolyser + balance-of-plant

In this section, an electrolyser cost of $450/kW is used with a reference current density of 500 mA cm^{-2}.[6] Therefore, the total electrolyser cost can be calculated as follows:

Total electrolyser cost ($) =

$$Power\ (kW) \times electrolyser\ unit\ cost\ (\$450/kW) = \quad \text{Eq. S14}$$

$$J \times S_{electrode} \times V_{cell} \times electrolyser\ unit\ cost\ (\$450/kW)$$

The capital costs for the **HOR|CEM|HCO_3^-** (7.2 $M), **OER|BPM|$HCO_3^-$** (14 $M), and **OER|AEM|$CO_2$** electrolysers (11 $M) varied because of the respective differences in cell potentials. The balance-of-plant capital costs were assumed to be 35% of the electrolyser capital costs.

2.2.4. Revenue, Profit, and NPV

The CO produced from each electrolyser was assumed to be sold at a constant price of $0.60/kg for a 20-year plant life. The yearly revenue for the three electrolyser pathways was 22 $M/year. The yearly profit for the **HOR|CEM|HCO_3^-**, **OER|BPM|HCO_3^-**, and **OER|AEM|CO_2** electrolysers were 13, 11, and 7.8 $M/year, respectively. The 20-year NPV for each technology was calculated using the spreadsheet developed by Jiao and coworkers.[4] The 20-year NPV results are as follows: **HOR|CEM|HCO_3^-** (57 $M); **OER|BPM|$HCO_3^-$** (39 $M), and **OER|AEM|$CO_2$** electrolysers (28 $M).

3. Energy consumption analysis (Sankey diagram)

Table S1. Input and output parameters from the energy analysis of the **OER|AEM|CO_2** and **HOR|CEM|HCO_3^-** electrolysers.

	HOR|CEM|HCO_3^-	**OER|AEM|CO_2**	**References**
Input parameters			
Voltage (V)	2.5	3	This work
CO_2 utilization (%)	40	20	This work
FE_{CO} (%)	50	90	This work
J (mA cm^{-2})	500		This work
CO_2 capture to form (bi)carbonate (KJ/mol CO_2)	10	13	[10]
CO_2 release energy from $CaCO_3$ (KJ/mol CO_2)	NA	178	[19]
Thermal energy efficiency	NA	78%	[19]
CO_2 pressurization energy (KJ/mol CO_2)	NA	20	[19]
H_2 energy consumption (KJ/mol H_2)	374	NA	[20]
Output parameters			
Energy cost for capturing and release CO_2 (KJ/mol CO_2)	13	258	
Full cell energy efficiency	26.8%	40.2%	
Electrolysis energy consumption (KJ/mol CO)	959.7	649.8	
Total Energy Consumption (KJ/mol CO)	**1358.7**	**1930.8**	

4. BPM and Nafion membrane

Anionic crossover from cathode to anode in a bicarbonate electrolyser causes a reduction in the flux of H^+ to the cathode because the total ionic flux is constrained by the current density. BPMs have been shown to limit crossover relative to cation exchange membranes because water splitting (which drives H^+) dominates at high current densities relative to co- and counter-ion transport.[21–23] Therefore, we

expected that protons are responsible for more ionic charge transport in the **OER|BPM|HCO_3^-** system than the **HOR|CEM|HCO_3^-** system. Because H^+ transport is related to *i*-CO_2 formation, we decided to test our hypothesis by measuring the difference in *i*-CO_2 released between the **OER|BPM|HCO_3^-** and **HOR|CEM|HCO_3^-** systems during constant current density electrolysis at 100 mA cm^{-2}. The results showed that the **OER|BPM|HCO_3^-** system produced more *i*-CO_2 than the **HOR|CEM|HCO_3^-** system (Table S2), which is consistent with our proposal regarding the H^+ transport mechanism. Moreover, the results suggest that differences in CO_2 supply to the cathode may be the cause of the different FE_{CO} values observed between the **OER|BPM|HCO_3^-** and **HOR|CEM|HCO_3^-** systems.

Table S2. *i*-CO_2 measured from the electrolyser with different membranes at 100 mA cm^{-2}.

	OER|BPM|HCO_3^-	**HOR|Nafion 212|HCO_3^-**
i-CO_2 (sccm) at 100 mA cm^{-2}, 1 atm	4.0 ± 0.5	3.7 ± 0.4

4. Supplementary figures

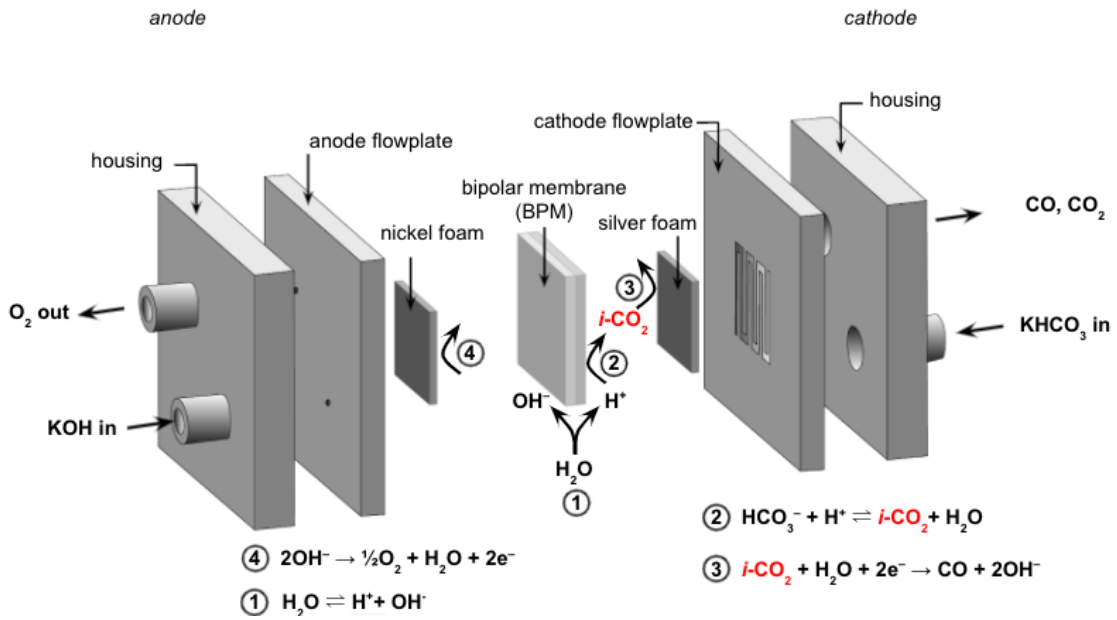

Figure S1. Illustration of the 'zero-gap' bicarbonate electrolyser used in this study. The bicarbonate electrolyser consists of serpentine cathode and anode flow plates that sandwich a nickel foam anode, a BPM, and a silver foam cathode. We define "i-CO_2" as a measure of the total amount of CO_2 that is generated within the electrolyser from acid-base reactions.

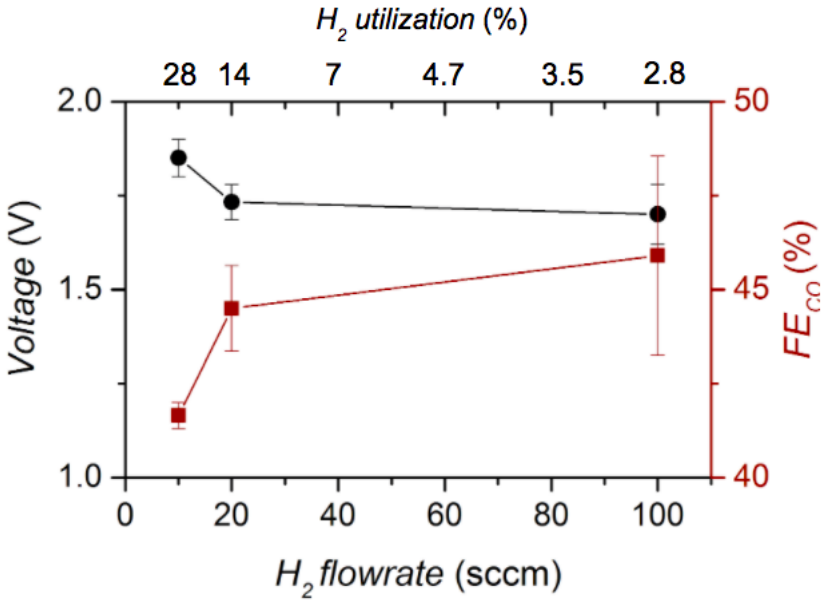

Figure S2. The impact of the H_2 flow rate on the cell voltage and FE_{CO} of the the **HOR|CEM|HCO_3^-** operated at a constant current density of 500 mA cm^{-2}.

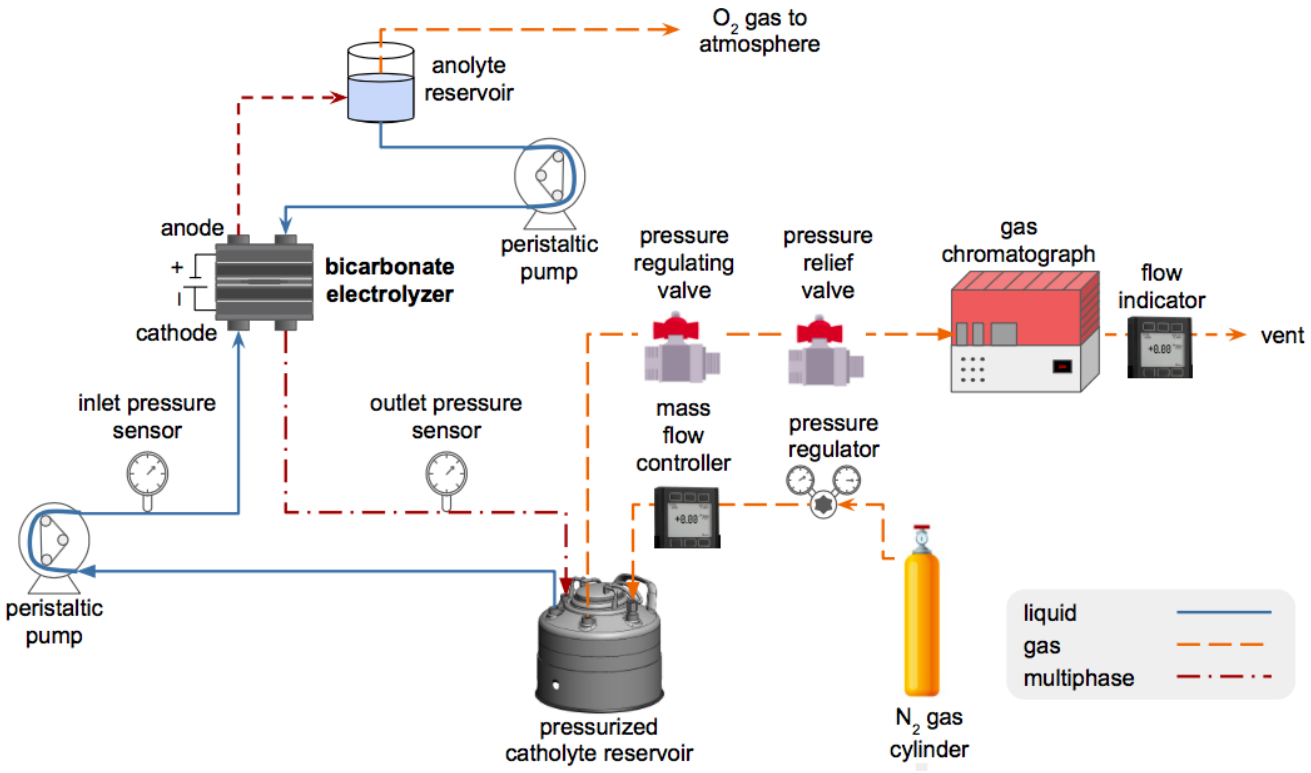

Figure S3. Schematic depiction of the pressurized bicarbonate electrolyser system. N_2 gas was used to control the pressure of the system, and the pressure value of the liquid feedstock was measured at

the inlet of the electrolyser by a pressure sensor. The flow rate of gas was controlled using a mass flow controller and the pressure was controlled using a pressure regulating valve. The final products were measured by a gas chromatography. No liquid CO2RR product was detected.

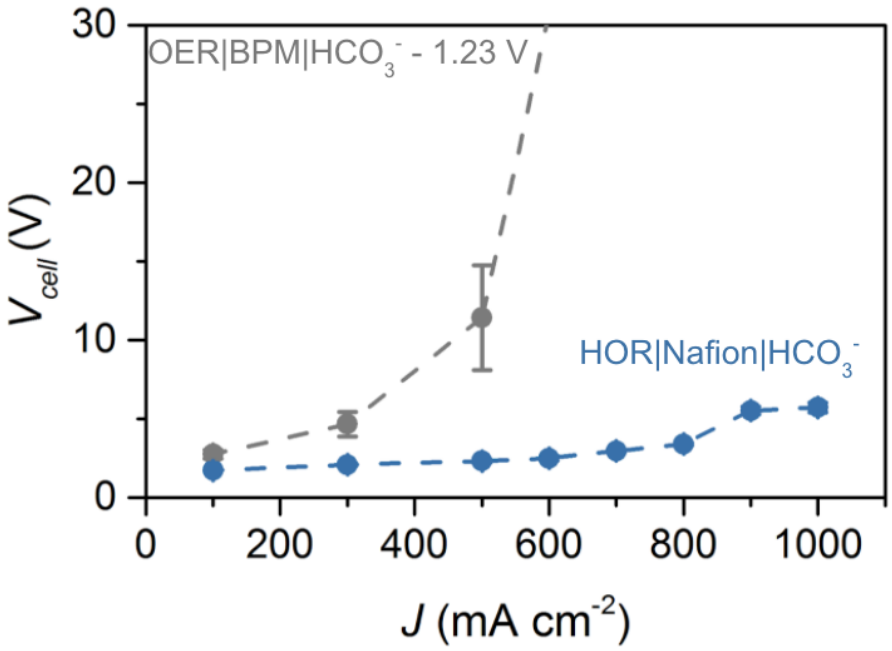

Figure S4. Modified V_{cell} values measured as a function of current density for the control system and the **HOR|CEM|HCO_3^-** with a Nafion membrane (25 μm). We subtracted the thermodynamic 1.23 V OER potential from the control system.

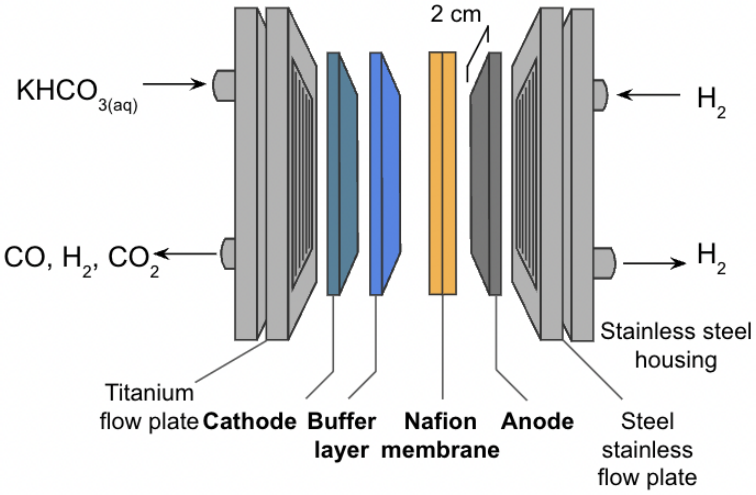

Figure S5. Schematic depiction of the HOR|CEM|HCO_3^- with a Nafion membrane (50 μm) with a buffer layer positioned between the Nafion membrane and silver foam cathode.The FE_{CO} increases from 47% to 71% at 100 mA cm^{-2} at 1.0 atm.

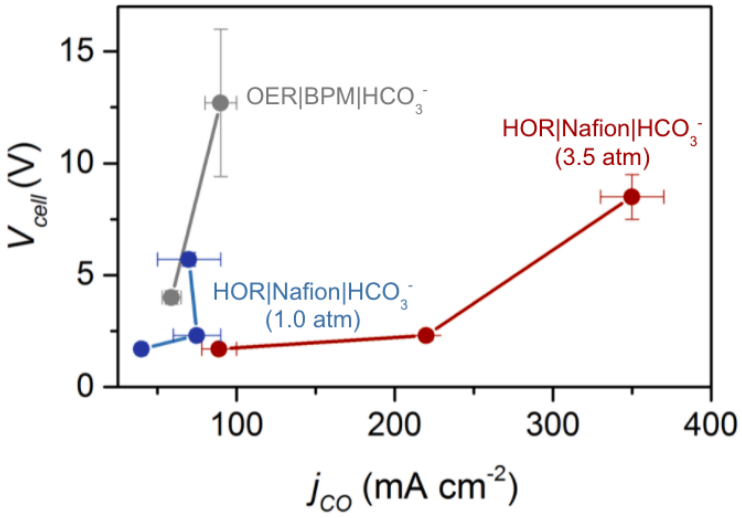

Figure S6. V_{cell} values measured as a function of partial current density for the control system, the **HOR|CEM|HCO$_3^-$** with a Nafion membrane (25 µm, 1.0 atm) and the **HOR|CEM|HCO$_3^-$** with a Nafion membrane (50 µm, 3.5 atm).

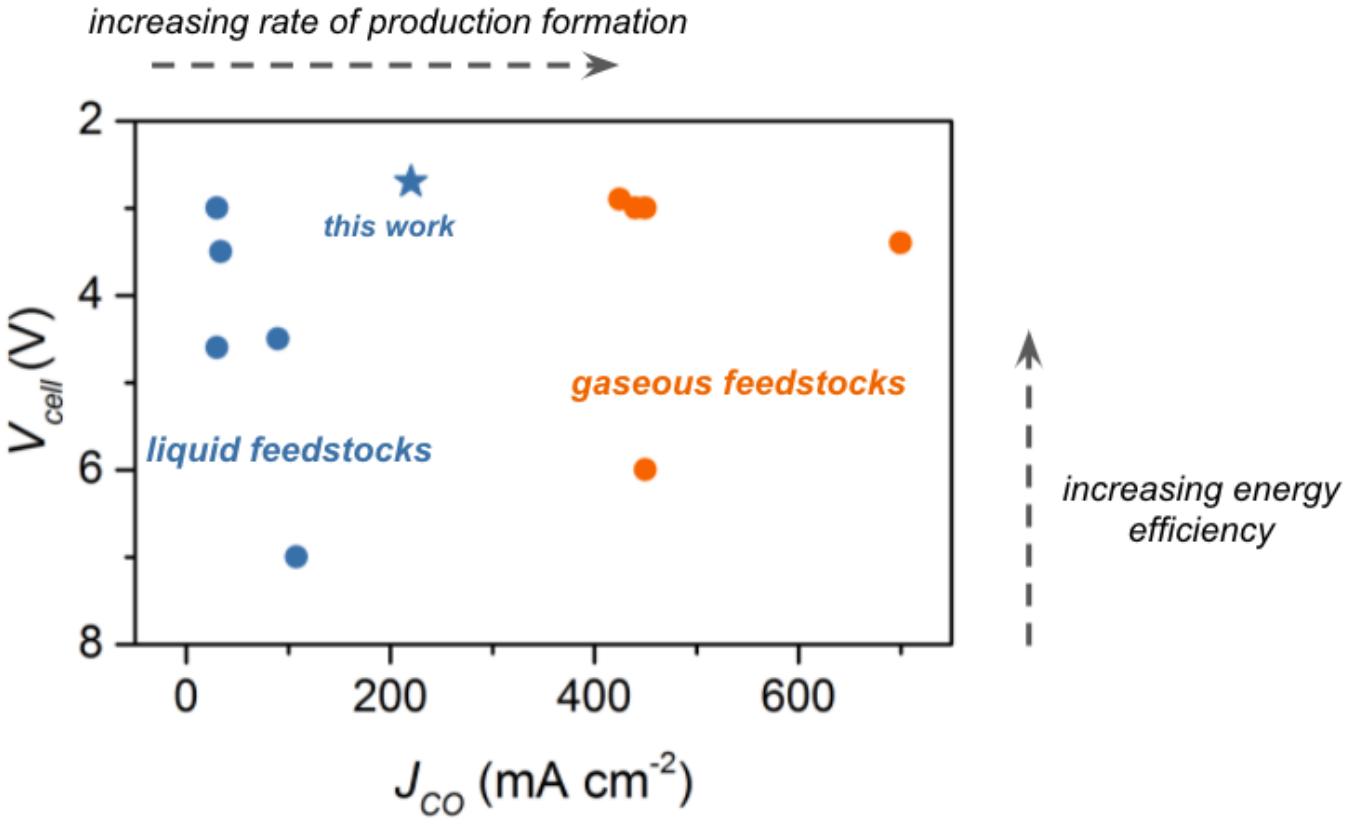

Figure S7. Literature current density and voltage values for reducing CO_2 using liquid (blue)[24–28] and gaseous feedstocks (orange)[29–33]. The star symbol represents the values reported in this work.

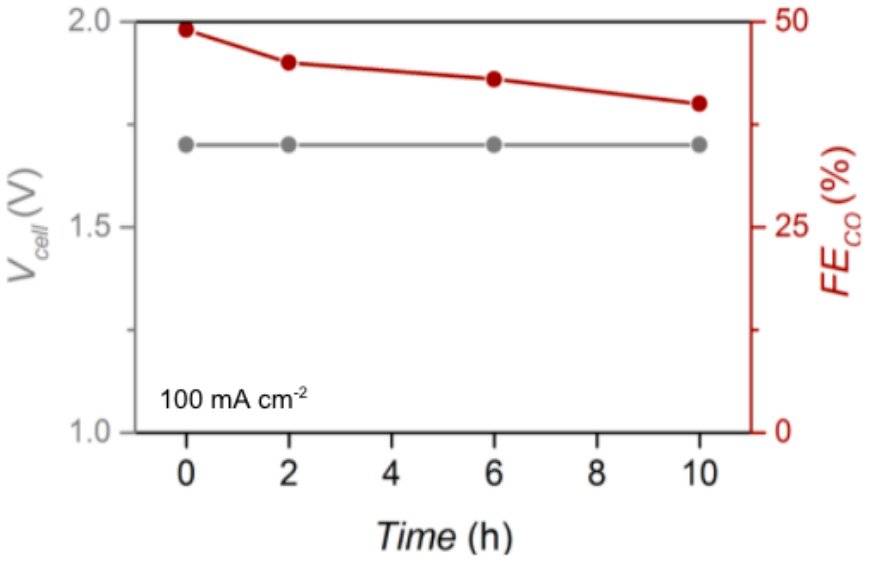

Figure S8. Voltage and FE_{CO} changes during 10 h electrolysis at 100 mA cm^{-2} (1.0 atm) for the HOR|CEM|HCO_3^- system. Cell voltage was stable at 1.7 V, and the membrane used in the cell is Nafion 212.

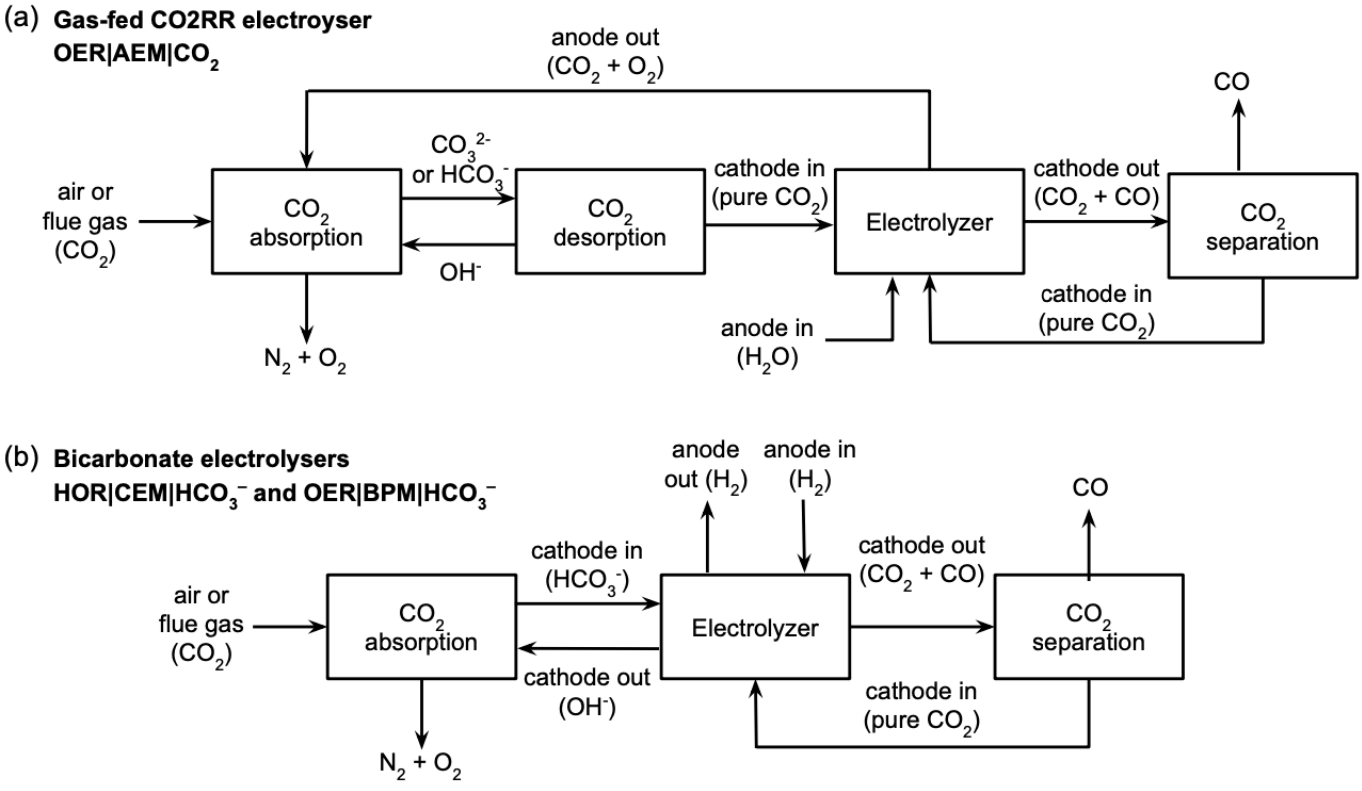

Figure S9. Process flow diagrams considered for the technoeconomic analysis of the three electrolyser architectures presented in this study. The gas-fed CO2RR electrolyser pathway (**OER|AEM|CO_2**) is represented in (a) with an additional CO_2 desorption step relative to the bicarbonate electrolyser pathway (**HOR|CEM|HCO_3^-** and **OER|BPM|HCO_3^-**) represented in (b).

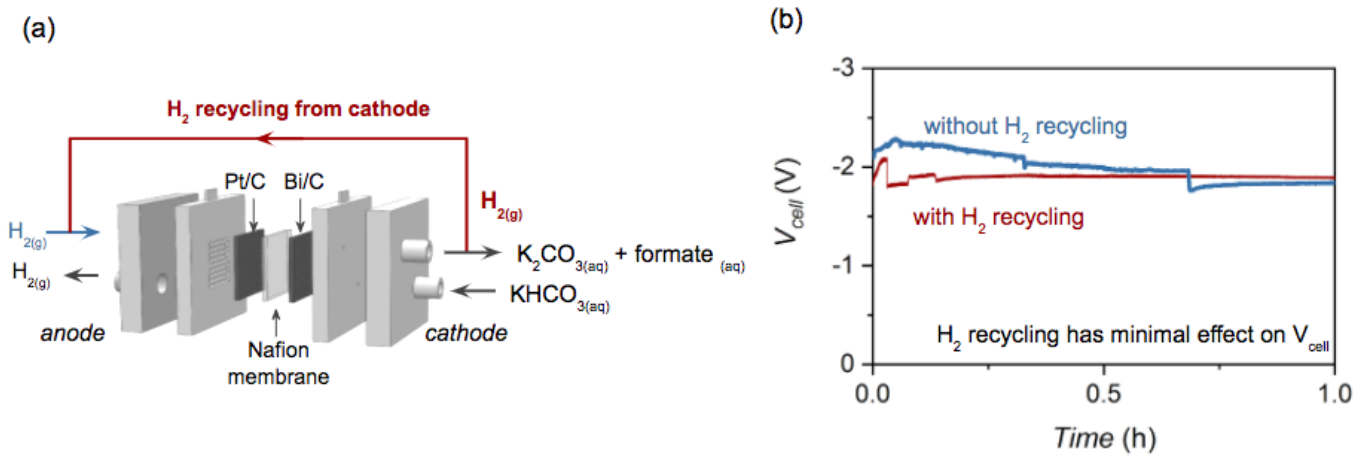

Figure S10. **H_2 produced at the cathode can be recycled to the anode compartment.** (a) Schematic diagram of the HOR|CEM|HCO_3^- system with a recycle stream that delivers H_2 produced at cathode to the anode for HOR. While this step would reduce the amount of virgin H_2 supplied to the system, the H_2 by-product would need to be separated from the CO product to avoid poisoning the platinized anode. We therefore modified the HOR|CEM|HCO_3^- system by changing the cathodic electrocatalyst from silver to bismuth in order to favor the formation of formate while suppressing the formation of CO (<100 ppm).[26] In these experiments, we directly recycled the cathodic product stream into the anode compartment with KOH solutions to remove the excessive *in situ* generated CO_2. Excess H_2 at the anode outlet can also be recycled to the anode inlet without further purification. (b) The V_{cell} profiles measured at a current density of 100 mA cm^{-2} for one hour with fresh H_2 feedstock and with recycled H_2 from the cathode. The H_2 recycling has minimal effect on the cell voltage over one hour of electrolysis, suggesting this recycling strategy is effective for reducing H_2 cost and increasing H_2 utilization.

5. References

(1) Salvatore, D. A.; Weekes, D. M.; He, J.; Dettelbach, K. E.; Li, Y. C.; Mallouk, T. E.; Berlinguette, C. P. Electrolysis of Gaseous CO_2 to CO in a Flow Cell with a Bipolar Membrane. *ACS Energy Lett.* **2018**, *3* (1), 149–154.

(2) Liu, M.; Mao, X.-A.; Ye, C.; Huang, H.; Nicholson, J. K.; Lindon, J. C. Improved WATERGATE Pulse Sequences for Solvent Suppression in NMR Spectroscopy. *J. Magn. Reson.* **1998**, *132* (1), 125–129.

(3) Weng, L.-C.; Bell, A. T.; Weber, A. Z. Modeling Gas-Diffusion Electrodes for CO_2 Reduction. *Phys. Chem. Chem. Phys.* **2018**, *20* (25), 16973–16984.

(4) Orella, M. J.; Brown, S. M.; Leonard, M. E.; Román-Leshkov, Y.; Brushett, F. R. A General Technoeconomic Model for Evaluating Emerging Electrolytic Processes. *Energy Technology* **2019**, 1900994.

(5) Jouny, M.; Luc, W.; Jiao, F. General Techno-Economic Analysis of CO_2 Electrolysis Systems. *Ind. Eng. Chem. Res.* **2018**, *57* (6), 2165–2177.

(6) Sisler, J.; Khan, S.; Ip, A. H.; Schreiber, M. W.; Jaffer, S. A.; Bobicki, E. R.; Dinh, C.-T.; Sargent, E. H. Ethylene Electrosynthesis: A Comparative Techno-Economic Analysis of Alkaline vs Membrane Electrode Assembly vs CO_2–CO–C_2H_4 Tandems. *ACS Energy Lett.* **2021**, *6* (3), 997–1002.

(7) Jeng, E.; Jiao, F. Investigation of CO_2 Single-Pass Conversion in a Flow electrolyser. *React. Chem. Eng.* **2020**, *5* (9), 1768–1775.

(8) Ma, M.; Clark, E. L.; Therkildsen, K. T.; Dalsgaard, S.; Chorkendorff, I.; Seger, B. Insights into the Carbon Balance for CO 2 Electroreduction on Cu Using Gas Diffusion Electrode Reactor Designs. *Energy Environ. Sci.* **2020**, *13* (3), 977–985.

(9) Larrazábal, G. O.; Strøm-Hansen, P.; Heli, J. P.; Zeiter, K.; Therkildsen, K. T.; Chorkendorff, I.; Seger, B. Analysis of Mass Flows and Membrane Cross-over in CO_2 Reduction at High Current Densities in an MEA-Type electrolyser. *ACS Appl. Mater. Interfaces* **2019**, *11* (44), 41281–41288.

(10) Welch, A. J.; Dunn, E.; DuChene, J. S.; Atwater, H. A. Bicarbonate or Carbonate Processes for Coupling Carbon Dioxide Capture and Electrochemical Conversion. *ACS Energy Letters* **2020**, *5* (3), 940–945.

(11) Rochelle, G. T.; Chen, E.; Oyenekan, B.; Sexton, A.; Davis, J.; Hilliard, M.; Veawab, A. CO_2 Capture by Absorption with Potassium Carbonate Third Quarterly Report 2006. *Austin, TX* **2006**.

(12) Abu-Zahra, M. R. M.; Niederer, J. P. M.; Feron, P. H. M.; Versteeg, G. F. CO_2 Capture from Power Plants: Part II. A Parametric Study of the Economical Performance Based on Mono-Ethanolamine. *Int. J. Greenhouse Gas Control* **2007**, *1* (2), 135–142.

(13) Raksajati, A.; Ho, M. T.; Wiley, D. E. Reducing the Cost of CO_2 Capture from Flue Gases Using Aqueous Chemical Absorption. *Ind. Eng. Chem. Res.* **2013**, *52* (47), 16887–16901.

(14) Ho, M. T.; Allinson, G. W.; Wiley, D. E. Factors Affecting the Cost of Capture for Australian Lignite Coal Fired Power Plants. *Energy Procedia* **2009**, *1* (1), 763–770.

(15) Hydrogen Shot https://www.energy.gov/eere/fuelcells/hydrogen-shot (accessed 2021 -08 -24).

(16) Haegel, N. M.; Margolis, R.; Buonassisi, T.; Feldman, D.; Froitzheim, A.; Garabedian, R.; Green, M.; Glunz, S.; Henning, H.-M.; Holder, B.; Kaizuka, I.; Kroposki, B.; Matsubara, K.; Niki, S.; Sakurai, K.; Schindler, R. A.; Tumas, W.; Weber, E. R.; Wilson, G.; Woodhouse, M.; Kurtz, S. Terawatt-Scale Photovoltaics: Trajectories and Challenges. *Science* **2017**, *356* (6334), 141–143.

(17) Steward, D.; Ramsden, T.; Zuboy, J. H2A Central Hydrogen Production Model, Version 3 User Guide (DRAFT). *National Renewable Energy Laboratory* **2012**.

(18) Rabinowitz, J. A.; Kanan, M. W. The Future of Low-Temperature Carbon Dioxide Electrolysis Depends on Solving One Basic Problem. *Nat. Commun.* **2020**, *11* (1), 5231.

(19) Keith, D. W.; Holmes, G.; St. Angelo, D.; Heidel, K. A Process for Capturing CO_2 from the Atmosphere. *Joule* **2018**, *2* (8), 1573–1594.

(20) Kauw, M.; Benders, R. M. J.; Visser, C. Green Methanol from Hydrogen and Carbon Dioxide Using Geothermal Energy And/or Hydropower in Iceland or Excess Renewable Electricity in Germany. *Energy* **2015**, *90*, 208–217.

(21) Li, Y. C.; Yan, Z.; Hitt, J.; Wycisk, R.; Pintauro, P. N.; Mallouk, T. E. Bipolar Membranes Inhibit Product Crossover in CO 2 Electrolysis Cells. *Advanced Sustainable Systems*. 2018, p 1700187. https://doi.org/10.1002/adsu.201700187.

(22) Blommaert, M. A.; Verdonk, J. A. H.; Blommaert, H. C. B.; Smith, W. A.; Vermaas, D. A. Reduced Ion Crossover in Bipolar Membrane Electrolysis via Increased Current Density, Molecular Size, and Valence. *ACS*

Appl. Energy Mater. **2020**, *3* (6), 5804–5812.
(23) Bui, J. C.; Digdaya, I.; Xiang, C.; Bell, A. T.; Weber, A. Z. Understanding Multi-Ion Transport Mechanisms in Bipolar Membranes. *ACS Appl. Mater. Interfaces* **2020**, *12* (47), 52509–52526.
(24) Li, T.; Lees, E. W.; Goldman, M.; Salvatore, D. A.; Weekes, D. M.; Berlinguette, C. P. Electrolytic Conversion of Bicarbonate into CO in a Flow Cell. *Joule* **2019**, *3* (6), 1487–1497.
(25) Lees, E. W.; Goldman, M.; Fink, A. G.; Dvorak, D. J.; Salvatore, D. A.; Zhang, Z.; Loo, N. W. X.; Berlinguette, C. P. Electrodes Designed for Converting Bicarbonate into CO. *ACS Energy Letters*. 2020, pp 2165–2173. https://doi.org/10.1021/acsenergylett.0c00898.
(26) Li, T.; Lees, E. W.; Zhang, Z.; Berlinguette, C. P. Conversion of Bicarbonate to Formate in an Electrochemical Flow Reactor. *ACS Energy Lett.* **2020**, 2624–2630.
(27) Li, Y. C.; Zhou, D.; Yan, Z.; Gonçalves, R. H.; Salvatore, D. A.; Berlinguette, C. P.; Mallouk, T. E. Electrolysis of CO2 to Syngas in Bipolar Membrane-Based Electrochemical Cells. *ACS Energy Lett.* **2016**, *1* (6), 1149–1153.
(28) Diaz, L. A.; Gao, N.; Adhikari, B.; Lister, T. E.; Dufek, E. J.; Wilson, A. D. Electrochemical Production of Syngas from CO2 Captured in Switchable Polarity Solvents. *Green Chemistry*. 2018, pp 620–626. https://doi.org/10.1039/c7gc03069j.
(29) García de Arquer, F. P.; Dinh, C.-T.; Ozden, A.; Wicks, J.; McCallum, C.; Kirmani, A. R.; Nam, D.-H.; Gabardo, C.; Seifitokaldani, A.; Wang, X.; Li, Y. C.; Li, F.; Edwards, J.; Richter, L. J.; Thorpe, S. J.; Sinton, D.; Sargent, E. H. CO2 Electrolysis to Multicarbon Products at Activities Greater than 1 A Cm-2. *Science* **2020**, *367* (6478), 661–666.
(30) Yin, Z.; Peng, H.; Wei, X.; Zhou, H.; Gong, J.; Huai, M.; Xiao, L.; Wang, G.; Lu, J.; Zhuang, L. An Alkaline Polymer Electrolyte CO_2 electrolyser Operated with Pure Water. *Energy Environ. Sci.* **2019**, *12* (8), 2455–2462.
(31) Verma, S.; Lu, X.; Ma, S.; Masel, R. I.; Kenis, P. J. A. The Effect of Electrolyte Composition on the Electroreduction of CO_2 to CO on Ag Based Gas Diffusion Electrodes. *Phys. Chem. Chem. Phys.* **2016**, *18* (10), 7075–7084.
(32) Endrődi, B.; Kecsenovity, E.; Samu, A.; Halmágyi, T.; Rojas-Carbonell, S.; Wang, L.; Yan, Y.; Janáky, C. High Carbonate Ion Conductance of a Robust PiperION Membrane Allows Industrial Current Density and Conversion in a Zero-Gap Carbon Dioxide electrolyser Cell. *Energy Environ. Sci.* **2020**, *13* (11), 4098–4105.
(33) Chen, Y.; Vise, A.; Klein, W. E.; Cetinbas, F. C.; Myers, D. J.; Smith, W. A.; Deutsch, T. G.; Neyerlin, K. C. A Robust, Scalable Platform for the Electrochemical Conversion of CO2 to Formate: Identifying Pathways to Higher Energy Efficiencies. *ACS Energy Lett.* **2020**, *5* (6), 1825–1833.